

# Correlation between the dynamic fracture surface energy $G_{ID}$ and the amount of created surface

**Jean-Benoît Kopp<sup>1,\*</sup>, Jean Schmittbuhl<sup>2</sup>, Jian Lin<sup>1</sup>, Christophe Fond<sup>1</sup>**

<sup>1</sup> ICube- 2 rue Boussingault, F67000 Strasbourg

<sup>2</sup> Ecole et Observatoire des Sciences de la Terre, 5 Rue René Descartes, F67000 Strasbourg

\* Corresponding author: jbkopp@unistra.fr

---

## Abstract

For rapid crack propagations, two kinds of material behavior have been observed. Typically, most materials show an increase of the fracture energy with the crack tip velocity. However, there do exist a few materials for which the fracture energy tends to decrease with the velocity [1, 2]. They are viscoplastic blend materials like polymers such as rubber toughened polymethylmethacrylate (RT-PMMA). For these materials, crack tips are seen to propagate at the same velocity whatever the loading rate is (or strain energy release rate). This critical velocity has been shown to be the crack branching velocity, at least at a macroscopic scale. Our study shows that the classical approach which considers that the amount of created surface during the propagation can be approximated as the sample thickness multiplied by the crack length is not appropriate. Indeed, this study shows that the exact fracture surface roughness has to be included in the amount of created surface in order to establish an intrinsic material fracture energy  $G_{ID}$ . As the fracture surface roughness depends on the scale at which the sample is observed, a self-affine model widely used for fracture surfaces is introduced [3, 4]. This statistical geometrical model of the fracture surface with two parameters, a Hurst exponent and a topothesy is shown to be effective and provides a better estimate of the intrinsic surface fracture energy.

**Keywords** Dynamic fracture, rapid crack propagation, polymers, energy release rate, self-affine analysis, Hurst exponent.

---

## 1. Introduction

Considering rapid crack propagation, two kinds of material behavior have been observed. On the one hand, there are materials for which the fracture energy increases with the crack tip velocity. Fracture velocity changes during the crack propagation when the released energy varies, i.e. the dynamic energy release rate  $G_{ID}$ . Practically, a difference of velocity before and after branching is observed and, for instance, the main crack propagates faster than the secondary cracks after branching [5-7]. On the other hand, there are materials for which the fracture energy tends to decrease with velocity. They are viscoplastic blend materials and typically polymers such as rubber toughened polymethylmethacrylate (RT-PMMA) or many semi-crystalline polymers. In these materials, crack tips are seen to propagate at the same macroscopic velocity whatever the macroscopic fracture energy in mode I sollicitation [1, 8, 9]. This velocity corresponds to the crack branching velocity, typically  $0.6C_r$ , where  $C_r$  is the Rayleigh wave speed. In the case of rapid crack propagations, as observed in [1], to maintain the propagation at the same macroscopic crack branching speed, the surface roughness evolves as a function of the available energy release rate  $G_{ID}$ . Below a minimal value of  $G_{ID}$ , cracks stop without any decrease of the crack tip velocity contrarily to the first kinds of materials. Crack arrest phases correspond to relatively smooth fracture surfaces and fracture surface roughness is seen to increase with the value of fracture energy at constant velocity. These observations confirm the aim of this study to explore the roughness of fracture surfaces as a function of the energy release rate  $G_{ID}$ . Moreover, classical consideration of the created surface such as the sample thickness times the crack length is not appropriate since several values can be obtained for the fracture energy at constant crack tip velocity. Evaluating the quantity of created surface is not simple since the surface roughness is correlated with the scale at which the sample is observed. Hence, validating the self-affine geometrical model would be of great

interest. The concept of self-affinity [10] of surface roughness has been described for many natural surfaces including fracture surfaces. This concept allows the introduction of the existence of a roughness exponent called the Hurst exponent [11] which is known to be unique and universal between 0.78 and 0.80 for many materials such as rocks [3, 4, 12] wood [13-15], steel [16-18] or polymers [19-21]. This study shows the interest of the self-affine geometrical model of fracture surface, with two parameters being the Hurst exponent and the topothesy.

## 2. Materials and methods

The general principle of Rubber Toughened (RT) reinforcement is to dissipate energy throughout the material through elastomer particles in contrast to pure amorphous polymers for which the energy dissipation is smaller and only located at the crack tip [22-31]. RT-PMMA consists of a PMMA matrix containing a volume fraction of approximately 20% of spherical elastomer particles of about 200nm in diameter. The elastomer particles are prepared separately and then mixed with PMMA in a fluid state at high temperatures. The glass transition temperature  $T_g$  of the matrix is 105°C while that of the elastomer particles is about -30°C. Fig. 1 presents sample characteristics for rapid crack propagation (RCP) tests.

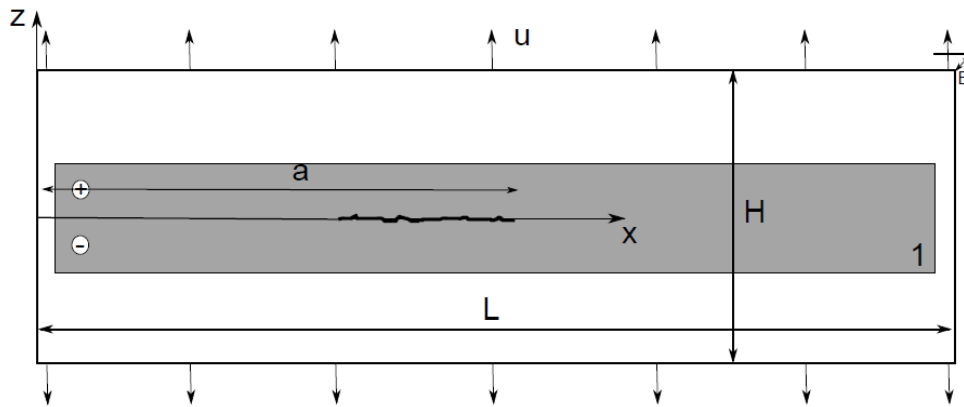


Figure 1. Schematic representation of the strip band geometry ( $L \approx 200\text{mm}$ ,  $25\text{mm} < H < 45\text{mm}$ ,  $B \approx 2\text{mm}$ ) uniformly loaded with imposed displacements  $u$  in mode I. A conducting layer (1-an Ag layer of approximately  $10\ \mu\text{m}$  is spread on the sample) used to record the crack tip position during propagation.

A conductive layer is sprayed onto the sample and the resistance evolution is recorded during the fracture, with a National Instrument USB-6351 data acquisition which ensures a  $1.25\ \text{MS}\cdot\text{s}^{-1}$  sampling rate. After calibration, fracture tip velocities are measured.

The strip band geometry allows a relatively simple mechanical analysis of the structure [32]. Samples are initially preloaded in tension using an Instron tensile testing machine equipped with a 150 kN force cell. A notch  $a_0 \approx 5/2 \cdot H$  is machined in the sample before loading. Crack propagation is then initiated by an impact of a razor blade at the tip of the notch. The entire test is performed at a quasi-constant temperature of 23°C.

An opto-mechanical stylus profilometer was used to characterize the *post-mortem* fracture surface of the RT-PMMA. A mechanical arm carrying a stylus is moved horizontally at constant speed (about  $1\ \text{mm}\cdot\text{s}^{-1}$ ) and subjected to a gravity force ensuring that the sapphire tip ( $\varphi = 5\ \mu\text{m}$ ) keeps in contact with the surface. Measurements are discretized along a grid ( $N_x, N_y$ ) with a mesh ( $\Delta_x, \Delta_y$ ). This technique is compatible with surface transparency which prevents the direct use of optical techniques. The present profilometer cumulates optical precision of the height measurement and mechanical description of the air/RT-PMMA interface (no penetration).

First of all, height measurements  $Z(X,Y)$  are used to build the topography of fracture surfaces. The chosen mesh grid is:  $\Delta_x = \Delta_y = 10\ \mu\text{m}$  with a resolution of  $2\ \mu\text{m}$ . Fracture maps show the surface

roughness during crack propagation, in particular during branching or crack arrest (see Fig. 2-3). Note that for RT-PMMA macroscopic fracture speed is observed to be constant even if the roughness changes [1]. Fig. 2 shows a perspective view of the fracture topography, before a branching zone.

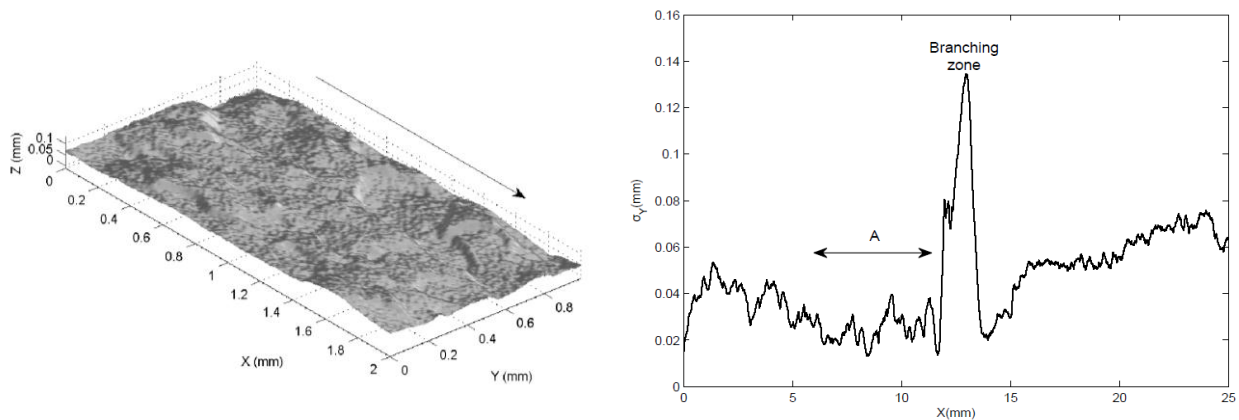


Figure 2. Topography of a fracture surface of RT-PMMA before a branching zone and standard deviation  $\sigma_y(x)$  of the height along the Y axis in function of the X axis which defines the stationary state (A) just before a branching zone.

This study also addresses the surface topography decrease just before a crack arrest in a sample of RT-PMMA (Fig. 3) when the fracture energy becomes too low for the crack to continue. A small cut is made to the samples in order to access crack arrests zones. To illustrate the variation of the surface roughness during crack propagation, the standard deviation  $\sigma_y$  (Eq. 1) of the height  $Z(X,Y)$  along the Y axis is calculated as a function of the X axis. The amplitude variation of  $\sigma_y$  is used to make the difference between stationary and non-stationary regimes. A stationary regime corresponds to quasi-constant fluctuations of  $\sigma_y$ . Fig. 2 and Fig. 3 show two stationary states before branching (A) and after branching (B):

- Regime A:  $\sigma_y$  amplitudes seem relatively constant just before a branching zone.
- Regime B:  $\sigma_y$  amplitudes seem relatively constant just before a crack arrest.

$$\sigma_y^2 = \frac{1}{N} \sum (h - \bar{h})^2 \quad (1)$$

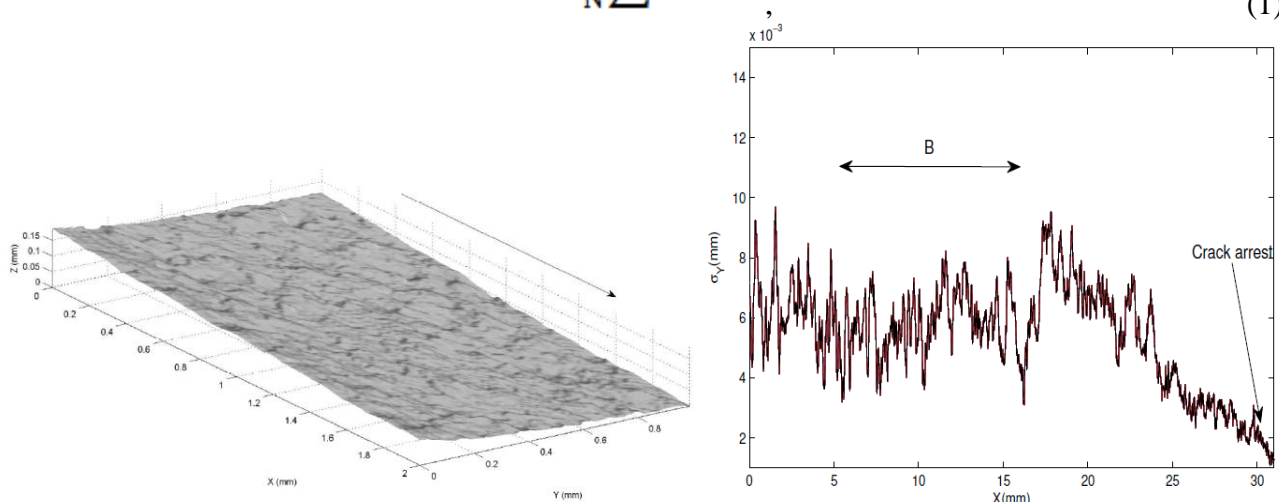


Figure 3. Topography of a fracture surface of RT-PMMA just before a crack arrest and standard deviation  $\sigma_y(x)$  of the height along the Y axis in function of the X axis which defines the stationary state (B) just before a crack arrest phase.

In order to estimate fracture surfaces a routine in Fortran was created with two estimating methods. The first method called “spherical convolution” consists to probe the experimental surface with an imaginary profilometer having a variable needle radius  $R_p$ . The second method called “sampling” consists in undersampling data, i.e. to keep a point every  $R_p$  (Fig. 4). Finally, this program computes the amount of developed fracture surface  $\mathcal{A}$  and developed lengths respectively along X and Y axis ( $l_x, l_y$ ).

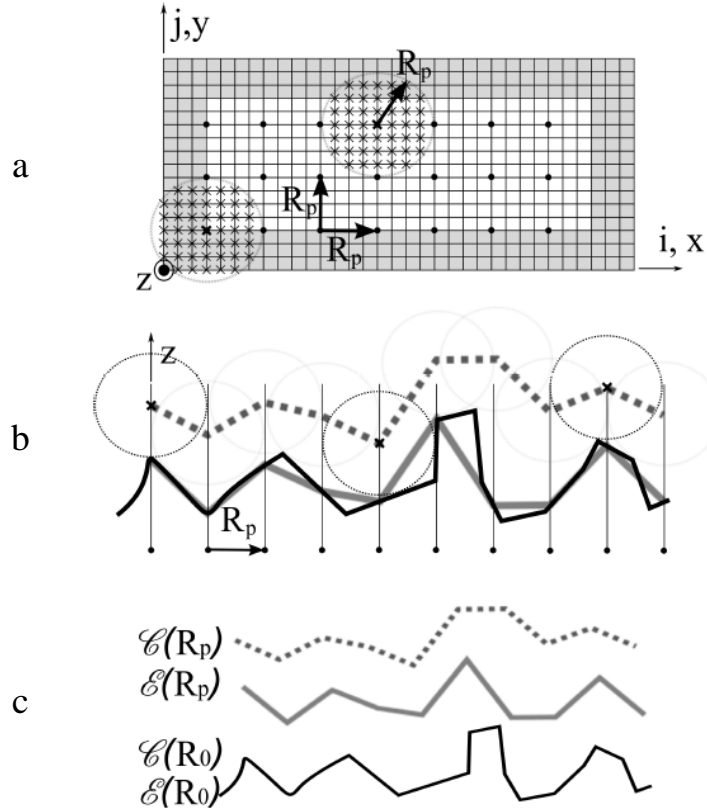


Figure 4. a-Top view of the synthetic profile b- “Spherical convolution” method and “sampling” method c-Profile of fracture surface obtained with the help of “spherical convolution” method or “sampling” method.

Finally, the concept of self-affinity introduced by Mandelbrot [10] is used to describe the roughness of fracture surfaces of RT-PMMA. It applies to surfaces that are statistically invariant under an affine transformation, such as:  $X \rightarrow \lambda_x.X$  ;  $Y \rightarrow \lambda_y.Y$  ;  $Z \rightarrow \lambda_z.Z$  with  $\lambda_x = \lambda_y$ ;  $\lambda_z = \lambda_x^\chi$  with  $\chi$ , the roughness exponent, or the Hurst exponent ( $0 < \chi < 1$ ). Today, there are various analytical techniques to analyze stationary and transient self-affinity. Root Mean Square (RMS), Maximum-Minimum (MM), Fourier Power Spectrum (FPS) and Averaged Wavelet Coefficient (AWC) methods which are used in this study are described in [4, 33-35]. The aim is to determine a self-affine geometrical model of the fracture surface from the estimates of the Hurst exponent and the topothesy  $l_r$  or the pre-factor  $C$ . The topothesy [35-38] which corresponds to the theoretical length scale over which the surface roughness has an average slope of  $45^\circ$  ( $\sigma(l_r)=l_r$ ) is calculated using the RMS method (Eq. 2):

$$\sigma(\Delta x) = C \cdot \Delta x^\chi \text{ with } C = l_r^{(1-\chi)}, \quad (2)$$

The energy release rate  $G_{Id}$  (Eq. 3) is computed assuming a classical Griffith energy balance accounting for inertial effects such as:

$$G_{Id} = \frac{\Delta W_{ext} - \Delta W_{ela} - \Delta K_{cin} - \Delta W_{dis}}{B\Delta a}, \quad (3)$$

where  $B$  is the thickness of the sample,  $\Delta a$  the crack length,  $W_{ela}$  the strain elastic energy,  $K_{cin}$  the kinetic energy,  $W_{ext}$  the work done by external forces and  $W_{dis}$  the bulk dissipated energy integrated over the entire structure. It has been largely assessed with optical techniques that Linear Elastic Fracture Mechanics (L.E.F.M.) formalism is valid for the dynamic fracture of amorphous polymers since the process zone is sufficiently confined [39, 40]. When the crack tip position  $a(t)$  during propagation and the initial stress state are known, the energy release rate  $G_{ID}$  may be calculated between two tip positions  $a$  and  $a+\Delta a$  by means of a transient dynamic finite element procedure, using the CAST3M software [41]. Dissipated energy, such as damping, does not involve nonlinear behavior in the process zone but only outside the process zone. Indeed, assuming L.E.F.M, the fracture toughness  $G_{Idc}$  accounts for non linearities in the process zone by setting  $G_{Idc} = G_{Id}$  for crack length increase. Since it has been shown that viscoelasticity is negligible for these experiments,  $W_{dis} = 0$  [42].

### 3. Results

During rapid crack propagation (RCP) tests, the macroscopic crack speed is quasi constant for a given specimen at a given temperature, whether branching occurs or not (Fig. 5). However, for a quasi-constant crack speed, several values of energy released rates have been recorded. The information given in the Table 1 highlights a striking difference of  $\langle G_{ID} \rangle$  for a measured same crack speed.

Table 1. Mean dynamic fracture energy values for cracks which branch ( $\langle G_{ID} \rangle_{max}$ ) and stop ( $\langle G_{ID} \rangle_{min}$ ).

$\langle G_{ID} \rangle_{min} (kJ/m^2)$	$\langle G_{ID} \rangle_{max} (kJ/m^2)$	$\langle G_{ID} \rangle_{max} / \langle G_{ID} \rangle_{min}$
$0.58 \pm 0.2$	$1.70 \pm 0.2$	$3.0 \pm 0.2$

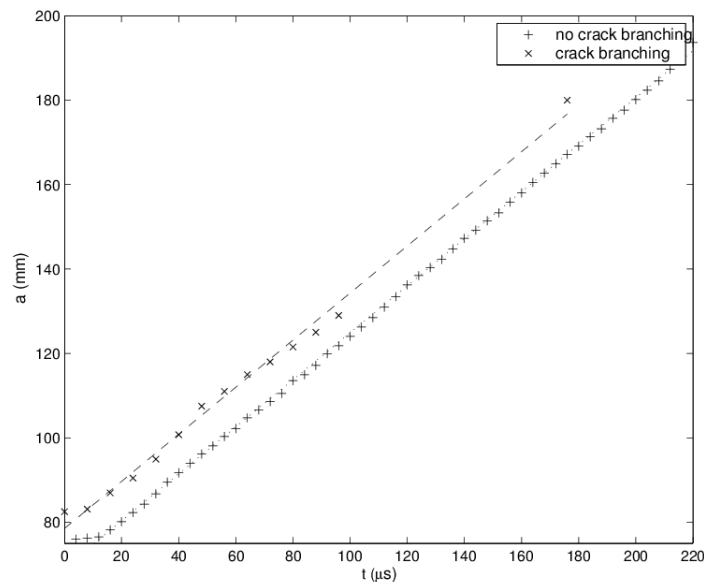


Figure 5. Crack lengths versus time in the case of crack branching and in the case of no macroscopic crack branching.

To quantify the differences of magnitudes of fracture surfaces between stationary states (A) and (B),

pre-factors are compared (Table 2). A significant difference of roughness is highlighted between the roughest and the smoothest surfaces observed on RT-PMMA samples.

Table 2. Pre-factors and topothesy calculated with RMS method before a branching zone (A) and a crack arrest (B).

	Pre-factor C (mm)	Topothesy $l_r$ (mm)	$C(A)/C(B)$
A	$10^{-1.84}$	$1 \cdot 10^{-4}$	2.4±0.2
B	$10^{-2.22}$	$9 \cdot 10^{-6}$	

Pre-factors and topothesy are calculated for each regime (A) and (B) for 10 samples of RT-PMMA. The ratio of  $C(A)$  to  $C(B)$  is equal to  $2.4 \pm 0.2$ . The self-affine geometrical model for stationary states (A) and (B) is defined with two parameters: the Hurst exponent and the topothesy. The results obtained by the two methods (RMS and MM) are shown in Fig. 6.

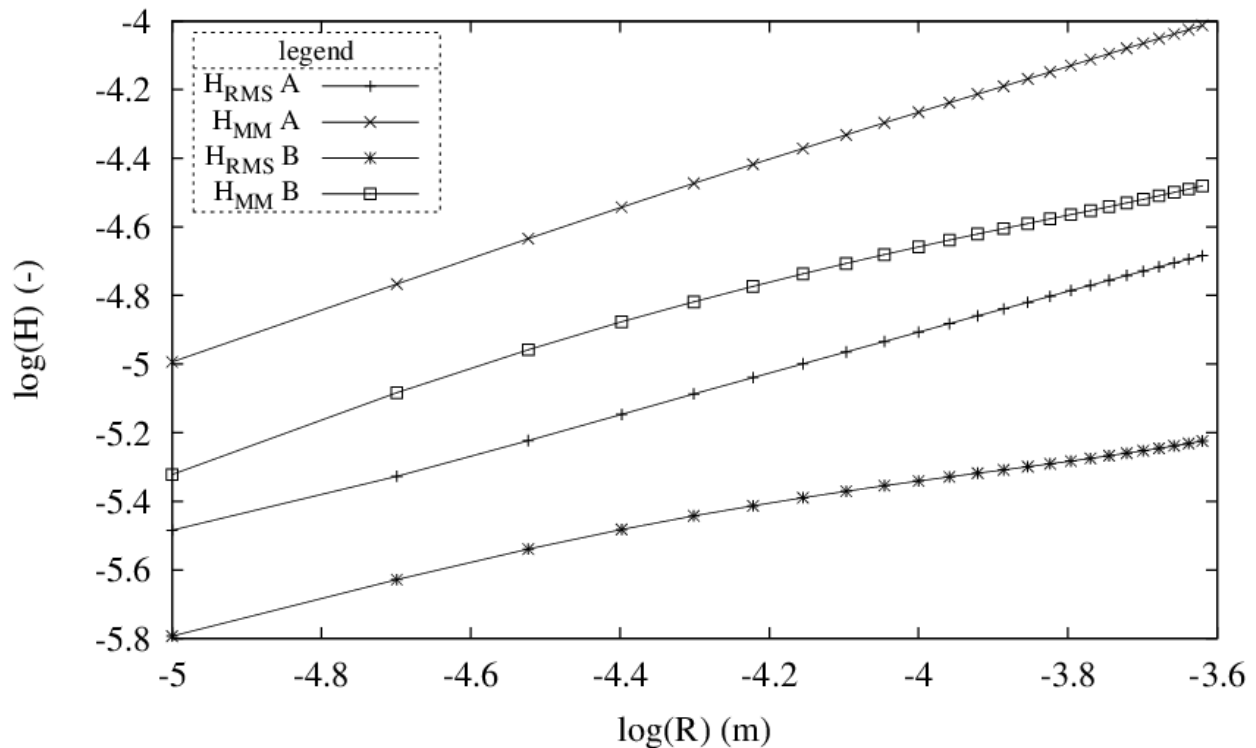


Figure 6. Statistical data analysis (RMS and MM) obtained by the characterization of RT-PMMA fracture surfaces (A and B).

The Hurst exponent is obtained from the average slope  $\beta$  of each curve in a log-log diagram with  $\beta = \chi$  for RMS and MM methods. All values of Hurst exponent which have been obtained are summarized in Table 3. The main observation is that the surface roughness of RT-PMMA follows a self-affine model in stationary regimes. In suggested stationary regimes (A and B) the self-affine model stays stable along the crack propagation with  $\langle \chi \rangle = 0.61 \pm 0.05$ . The average value of the Hurst exponent  $\langle \chi \rangle$  was calculated using the analysis of 10 profiles.

Table 3. Roughness exponent of RT-PMMA fracture surfaces for stationary states A and B.

Methods	RMS	MM
$\chi(A)$	0.54	0.60
$\chi(B)$	0.56	0.62

Furthermore, a decrease of the prefactor and the topothesy was observed between A and B states (Table 2). This corresponds to a significant decrease of surface roughness. Contrary to the pre-factor and the topothesy, the Hurst exponent stays stable between the two stationary regimes. The interest of analyzing the pre-factor and the topothesy provides an estimate of the difference of fracture surfaces between the two domains. Fig. 7 presents the quantity of developed surface for “spherical convolution” and “sampling” methods for stationary regimes (A) and (B). The amount of developed surface in domain (B) is significantly lower than the amount of developed surface in domain (A).

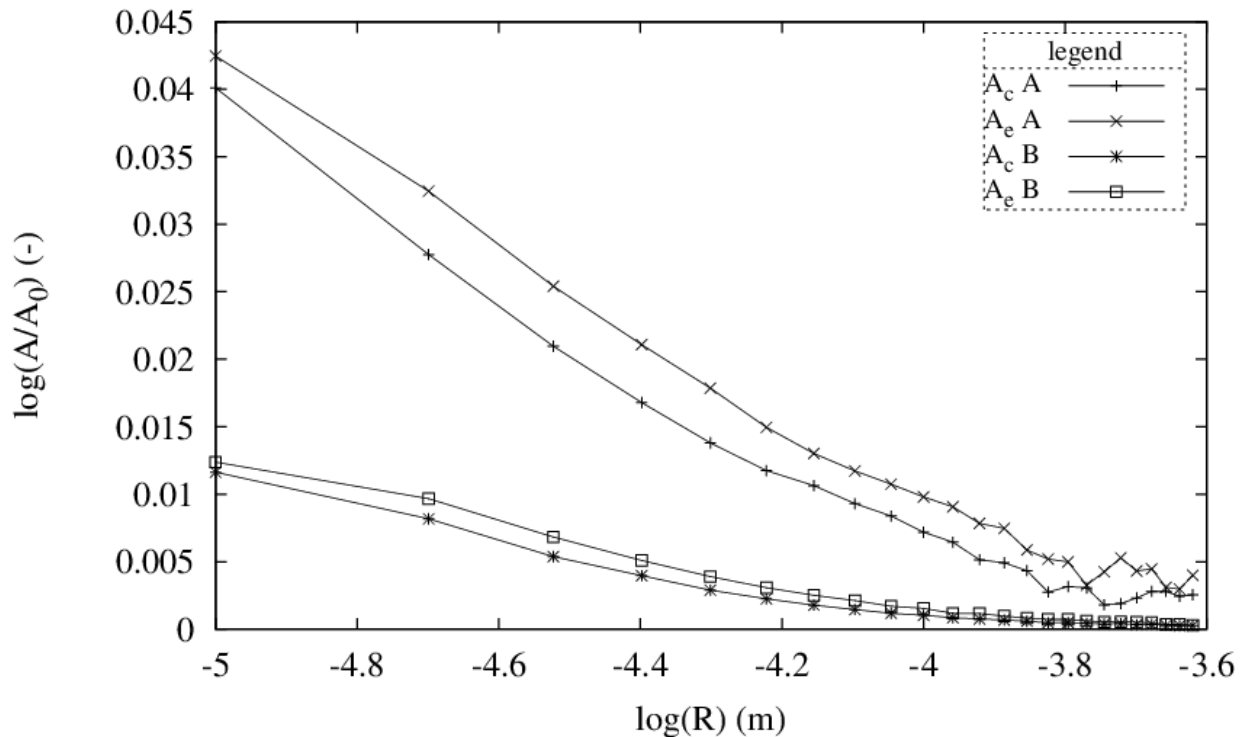


Figure 7. Total fracture surface for “spherical convolution” method (c) or “sampling” method (e) for stationary regimes (A) and (B).

Whatever the method, “spherical convolution” or “sampling”, the amount of developed surface which are calculated is relatively similar. The choice of the method thus is indifferent on the result.

#### 4. Discussion and conclusions

Using an dynamic L.E.F.M. approach, RT-PMMA samples have revealed a “loss” of  $G_{ID}$  unicity which is related to  $B\Delta a$  (Eq. 3) at a crack tip velocity of approximately  $0.6C_r$ . Indeed, maximum values of fracture energy have been shown to vary up to  $3.0 \pm 0.2$  times the minimum. The results suggest that differences of  $G_{ID}$  exist and are associated to the RMS of the fracture surface  $\sigma_y$ . In this article the roughness of fracture surfaces obtained from the analysis of *post-mortem* surfaces, has been quantified with Hurst exponents and pre-factors ratios during stationary regimes (A and B) before and after branching. Surfaces considered as inaccessible, either because of the profilometric technique ( $5\mu\text{m}$  sapphire radius tip) or because of local branches (sub-surfaces), are neglected in this study. However it is observed that the amount of fracture of inaccessible surface seems

negligible compared to the accessible surface. It is shown that a crack creates  $2.4 \pm 0.2$  times more surfaces before a branching zone than before a crack arrest. In addition, the self-affine model allows one to say that the surface roughness could be considered as statistically invariant under an affine transformation. Evidently the model could lose its validity below the micrometric scale, i.e. resolution scale. The “loss” of  $G_{ID}$  unicity at approximately  $0.6C_r$  can therefore be associated with the amount of created fracture surface even if the quantification of  $\mathcal{A}$  is practically fastidious.  $G_{ID}$  is calculated as a function of the created projected fracture surface ( $B\Delta a$ ) on the average fracture plane. In the case of rubber toughened polymer, and most probably semi-crystallines, experiments thus show that it would be pertinent to correct the real area of the crack surface  $\Delta\mathcal{A}/\Delta\mathcal{A}_0$  with  $\Delta\mathcal{A}_0=B\Delta a$  the projected area and  $\Delta\mathcal{A}$  the real surface. For these kinds of materials it would be necessary to multiply  $G_{ID}$  by  $\Delta\mathcal{A}/\Delta\mathcal{A}_0$ . Finally, the determination of the Hurst exponent ( $\chi=0.61 \pm 0.05$ ) independently of the fracture domain (A or B) supports the universality of the self-affine scaling of fracture surface for quasi-2D sample geometries. The self-affine geometrical model with two parameters (Hurst exponent and pre-factor or topothesy), shows its effectiveness in this type of study. However, the single Hurst exponent is no longer sufficient, by itself, to describe all the regimes encountered and, more precisely, with these kinds of rubber toughened polymers.

### References

- [1] C. Fond, R. Schirrer, Dynamic fracture surface energy and branching instabilities during rapid crack propagation in rubber toughened pmma, Notes au C.R.A.S., Series IIb 329 (2001a) 195–200.
- [2] C. Fond, R. Schirrer, Influence of crack speed on fracture energy in amorphous and rubber toughened amorphous polymers, *Plastics, Rubber and Composites* 30 (2001b) 116–124.
- [3] J. Schmittbuhl, S. Gentier, S. Roux, Field measurements of the roughness of fault surfaces, *Geophysical research letter* 20 (1993) 639–641.
- [4] J. Schmittbuhl, F. Schmitt, S. C., Scaling invariance of crack surfaces, *Journal of geophysical research* 100 (1995) 5953–5973.
- [5] J. G. Williams, Visco-elastic and thermal effects on crack growth in pmma, *International Journal of Fracture* 8 (1972) 393–401.
- [6] A. Kobayashi, N. Ohtani, M. Munemura, Dynamic stress intensity factors during viscoelastic crack propagation at various strain rates, *Journal of Applied Polymer Science* 25 (1980) 2789–2793.
- [7] W. Döll, Application of an energy balance and an energy method to dynamic crack propagation, *International Journal of Fracture* 12 (1976) 595–605.
- [8] J. Scheibert, C. Guerra, F. Celarie, D. Dalmas, D. Bonamy, Brittle-quasibrittle transition in dynamic fracture: An energetic signature, *Phys. Rev. Lett.* 104 (2010) 045501–1–045501–4.
- [9] E. Sharon, J. Fineberg, Confirming the continuum theory of dynamic brittle fracture for fast cracks, *Nature* 397 (1999) 333–335.
- [10] B. Mandelbrot, *The fractal geometry of nature*, W.H.Freeman and Company (NewYork) (1982).
- [11] K. Maloy, A. Hansen, E. Hinrichsen, S. Roux, Experimental measurements of the roughness of brittle cracks, *Phys. Rev. Lett.* 68 (1992) 213–215.
- [12] J. M. Lopez, J. Schmittbuhl, Anomalous scaling of fracture surfaces, *Physical Review E* 57 (1998) 6405–6408.
- [13] S. Morel, J. Schmittbuhl, J. M. Lopez, G. Valentin, Anomalous roughening of wood fractured surfaces, *Phys. Rev. E* 58 (1998) 6999–7005.
- [14] G. Mourot, S. Morel, G. Valentin, Comportement courbe-r d’un matériau quasi-fragile (le bois): Influence de la forme des spécimens d’essai, *Colloque MATERIAUX 2002* (2002).
- [15] L. Ponson, D. Bonamy, H. Auradou, G. Mourot, S. Morel, E. Bouchaud, C. Guillot, J. Hulin, Anisotropic self-affine properties of experimental fracture surfaces, *International Journal of fracture* 140 (1992) 27–37.
- [16] B. Mandelbrot, D. Passoja, A. J. Paulay, Fractal character of fracture surfaces of metals, *Nature* 308

- (1984) 721–722.
- [17] J. P. Bouchaud, E. Bouchaud, G. Lapasset, J. Planès, Models of fractal cracks, *Physical review letters* 71 (1993a) 2240–2243.
- [18] E. Bouchaud, G. Lapasset, J. Planès, S. Naveos, Statistics of branched fracture surfaces, *Phys. Rev. B* 48 (1993b) 2917–2928.
- [19] F. Lapique, P. Meakin, J. Feder, T. Jassang, Self-affine fractal scaling in fracture surfaces generated in ethylene and propylene polymers and copolymers, *Journal of Applied Polymer Science* 86 (2002) 973–983.
- [20] C. Guerrero, E. Reyes, V. Gonzalez, Fracture surface of plastic materials: the roughness exponent, *Polymer* 43 (2002) 6683–6693.
- [21] M. Hinojosa, V. Gonzalez, J. Sanchez, U. Ortiz, Scaling properties of the fracture surfaces of a crystalline polymer, *Polymer* 45 (2004) 4829–4836.
- [22] P. A. Lovell, M. M. Sherratt, R. J. Young, *Mechanical Properties and Deformation Micromechanics of Rubber-Toughened Acrylic Polymers*, 1996.
- [23] C. Fond, Cavitation criterion for rubber materials: A review of void-growth models, *Journal of Polymer Science Part B: Polymer Physics* 39 (2001) 2081–2096.
- [24] C. Fond, R. Schirrer, Renforcement des polymères - mécanismes et modélisations de la cavitation., in: *Physique des polymères à l'état solide*, volume 17, 2006, pp. 167–208.
- [25] O. Julien, P. Béguelin, L. Monnerie, H. H. Kausch, Loading-rate dependence of the fracture behavior of rubber-modified poly(methyl methacrylate), in: *Toughened Plastics II*, 1996, pp. 233–249.
- [26] C. B. Bucknall, R. R. Schmith, Stress-whitening in high-impact polystyrenes, *Polymer* 6 (1965) 437–446.
- [27] H. Keskkula, M. Schwarz, D. R. Paul, Examination of failure in rubber toughened polystyrene, *Polymer* 27 (1986) 211–216.
- [28] G. Dagli, A. Argon, R. Cohen, Particle-size effect in craze plasticity of high-impact polystyrene, *Polymer* 36 (1995) 2173–2180.
- [29] R. Borggreve, R. Gaymans, J. Schuijjer, J. Ingen Housz, Brittle-tough transition in nylon-rubber blends: effect of rubber concentration and particle size, *Polymer* 28 (1987) 1489–1496.
- [30] R. Borggreve, R. Gaymans, J. Schuijjer, Impact behaviour of nylon-rubber blends: 5. influence of the mechanical properties of the elastomer, *Polymer* 30 (1989) 71–77.
- [31] C. He, A. Donald, Morphology of a deformed rubber toughened poly(methyl methacrylate) film under tensile strain, *Journal of Materials Science* 32 (1997) 5661–5667.
- [32] F. Nilsson, Dynamic stress-intensity factors for finite strip problems, *International Journal of Fracture* 8 (1972) 403–411.
- [33] A.-L. Barabasi, H. E. Stanley, *Fractal concepts in surface growth*, Cambridge university press edition, 1995.
- [34] P. Meakin, *Fractals: Scaling and growth far from equilibrium*, Cambridge university press edition, 1998.
- [35] T. Candela, F. Renard, M. Bouchon, A. Brouste, D. Marsan, J. Schmittbuhl, C. Voisin, Characterization of fault roughness at various scales: Implications of three-dimensional high resolution topography measurements, *Pure and Applied Geophysics* (2009) 1817–1851.
- [36] I. Simonsen, D. Vandembroucq, S. Roux, Wave scattering from self-affine surfaces, *Phys. Rev. E* 61 (2000) 5914–5917.
- [37] J. Schmittbuhl, G. Chambon, A. Hansen, M. Bouchon, Are stress distributions along faults the signature of asperity squeeze, *Geophysical Research Letters* 33 (2007) L13307.
- [38] J. Schmittbuhl, A. Steyer, L. Jouniaux, R. Toussaint, Fracture morphology and viscous transport, *International Journal of Rock Mechanics and Mining Sciences* 45 (2008) 422–430.
- [39] J. F. Kalthoff, On the measurement of dynamic fracture toughnesses? A review of recent work, *International Journal of Fracture* 27 (1985) 277–298.
- [40] Bohme, W., Kalthoff, J. F., On the quantification of dynamic in impact loading and the practical application for kid-determination, *J. Phys. Colloques* 46 (1985) C5–213–C5–218.
- [41] Castem software: <http://www-cast3m.cea.fr/>
- [42] C. Fond, Endommagement des polymères "choc": modélisations micromécaniques et comportements à la rupture, *Habilitation à diriger des recherches en mécanique des solides*, Université Louis Pasteur de Strasbourg, 2000.